# Optimization of Processing and Properties of Medical-Grade Nitinol Wire

Pelton, DiCello, Miyazaki

Proceedings of the Int'l Conference on Shape Memory and Superelastic Technologies
SMST-2000
(eds.) S. Russell, A. Pelton

2000

# OPTIMIZATION OF PROCESSING AND PROPERTIES OF MEDICAL-GRADE NITINOL WIRE

**Alan R. Pelton,[1] John DiCello,[1] and Shuichi Miyazaki[2]**

[1]*Cordis Corporation - Nitinol Devices & Components*
*47533 Westinghouse Drive, Fremont CA 94539*

[2]*Institute of Materials Science, University of Tsukuba*
*Tsukuba, Ibaraki 305-3573, Japan*

## ABSTRACT

The purpose of this paper is to review the current processing and resultant properties of standard Nitinol wire for guidewire applications. Optimized Ti-50.8Ni (at.%) wire is manufactured according to industry standards by precise control of the composition, cold work, and continuous *strain-age* annealing. The first part of this paper will provide the key attributes of medical-grade Nitinol wire. Mechanical properties of this wire are reported from –100 to 200°C to demonstrate the effects of test temperature and to establish the concept of a *superelastic window*. It will be shown that within this window (0–60°C), the plateau stresses are linearly related to test temperature. The second part of this paper will demonstrate the time and temperature effects required to shape-set medical devices from the as-received Nitinol wire. It will be shown that these additional aging treatments can be used as a potent tool to fine tune transformation temperatures and, hence, mechanical properties. The third section will review fatigue properties of processed wire under various conditions pertinent for the medical-device industry.

## INTRODUCTION

The growth of Nitinol in the medical industries has exploded in the past 10 years. Patients and care providers have encouraged the transition from traditional, open-surgical procedures that require long hospital stays to less-invasive techniques, which are often performed in outpatient facilities [1]. This demand for minimally invasive procedures has allowed novel instrumentation and implants to be designed by engineers and physicians. An increasing number of these devices use Nitinol as the critical component. Examples of these medical applications are richly illustrated in companion articles in this volume, and range from endoscopic instruments to implants such as stents and filters [2–4].

Since the discovery of the shape memory effect in TiNi alloys in the 1960s, metallurgists have investigated methods to control transformation temperatures and mechanical properties through

alloying additions, improved melting practices, and thermomechanical processing (see, for example, References 5 and 6). The production of many thousands of kilometers of wire for such diverse products as cellular telephone antennas, eyeglass frame components, guidewires, undergarment supports, and orthodontic archwires profoundly influenced the acceptance of Nitinol in the marketplace. These commercial opportunities have allowed Nitinol suppliers to focus on improving processes for a few standard alloys rather than pursuing myriad boutique alloys with niche applications. The composition and processes have been refined so that, for example, the transformation temperature in final products is routinely controlled to within ± 3°C. More recently, the availability of seamless tubing and sheet have provided designers with additional tools to solve engineering problems. Furthermore, microfabrication techniques, such as laser machining and photoetching, have also contributed to the growth of miniature devices made from Nitinol [7,8]. Accordingly, Nitinol properties have become very predictable, which is a basic requirement of design engineers. As the Nitinol industry has matured over the past two decades, terms such as *shape memory*, *superelasticity*, *recovery forces*, *plateau stresses*, and *transformation temperatures* are now recognized by more than just a select few metallurgical specialists.

The purpose of this article is to review the processing and resultant properties of Ti-50.8Ni (at.%) wire that has been manufactured for medical guidewire applications. These properties will be shown to be a function of test temperature to illustrate the concept of a *superelastic window*. The effects of time and temperature required to shape set medical devices from the as-received Nitinol wire will also be discussed in detail. It will be shown that these additional aging treatments can be used as a potent tool to fine tune transformation temperatures and hence, mechanical properties. Fatigue resistance, which is a key property of medical devices, will also be discussed.

## PROCESSING

Optimization of the superelastic properties of Nitinol for a specific product is achieved through a combination of cold work and heat treatment. The first step in optimizing the thermomechanical treatments of wire and tubing products is to draw the material through a series of dies to achieve 30 to 50% reduction in cross-sectional area [9]. Continuous *strain annealing* ensures that the entire spool of wire will be processed with identical thermomechanical treatment, resulting in a product with uniform properties from end to end. Figure 1 shows a schematic of a typical continuous strain straightening process line.

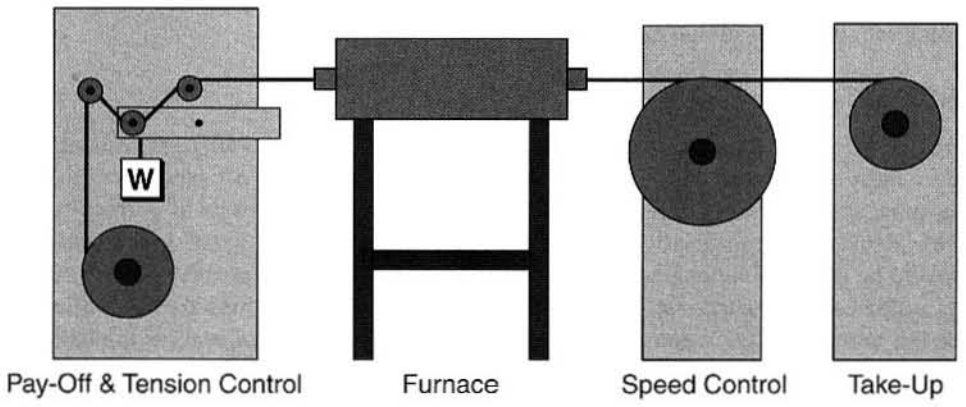


*Figure 1 Schematic diagram of a continuous strand of annealing equipment for optimized production of Nitinol superelastic wire.*

Continuous strand straightening usually occurs in a temperature range of 450 to 550°C under a stress of 35 to 100 MPa. As the wire moves into the heat zone, it will initially want to shrink in length and grow in diameter due to the Shape Memory Effect (SME) not suppressed by the cold work of the drawing process (springback). As the wire temperature rapidly increases, its strength will drop and with the applied strain will straighten the wire. Depending on the magnitude of the strain, the wire diameter may also reduce slightly. In the continuous process, it is difficult to measure the active strains during straightening as they occur inside the furnace. However, the following vertical straightening example can help define the strains operating during the continuous process. During vertical straightening of discreet lengths of wire, the wire is heated via electrical resistance and is, therefore, exposed to make visible measurements. As a 1.5 mm diameter wire was being electrically straightened, it showed a maximum springback of 1.2% during heating and a 2.4% extension strain at the end of the straightening cycle. Similar strains would be expected with the continuous strain straightening method.

Straightness, mechanical properties, and the active $A_f$ are all affected by the speed and temperature parameters of the straightening process. As with all thermally activated processes, time-at-temperature controls the final properties of the wire. More time-at-temperature softens the wire and moves its mechanical properties toward a fully annealed product while short times leave the material closer to the high-strength, cold-worked state. A balance must be developed between these two extremes to optimize the superelastic properties. The requirements of the final product will help define the process parameters. A high-torqueable guidewire may require slower speeds than a high-strength wire that has a table-roll straightness requirement. Additional speed and temperature adjustments may be necessary to meet any active $A_f$ requirements as well (see discussions below).

## PROPERTIES

In this section we will document the mechanical properties from –100 to 200°C to illustrate how test temperature affects performance. Furthermore, since many wire and tubing products are given additional thermal shape setting, we will establish the effects of aging time and temperature treatments on transformation and mechanical properties.

### EFFECTS OF TEST TEMPERATURE

The tensile curves shown in Figure 2 illustrate that the mechanical behavior of Nitinol varies greatly from –100 to 150°C. In these tests, wires with an $A_s$ of –22°C and $A_f$ of 11°C were pulled to 6% strain, unloaded to zero stress, and then pulled to failure. At the lowest test temperatures, the wires are martensitic, and the high residual strains are fully recovered by heating above $A_f$ after 6% strain. From about 0 to 100°C, the tensile curves exhibit superelastic *flags*, and we note that it becomes more difficult to stress induce martensite as the test temperature increases. Along with the increase in the plateau stresses, the permanent set also increases with temperature. The tensile behavior at 100°C, with a high permanent set but with a well-defined unloading curve, indicates that deformation is accommodated by a combination of stress-induced martensite and conventional plasticity. Above 150°C, however, the wire deforms by plastic mechanisms rather than martensitic transformations, which results in a linear unloading curve. The temperature where it is too difficult to stress induce martensite is defined as $M_d$; in the present case, $M_d$ is between 100 and 150°C.

The effects of test temperature on the tensile curves shown in Figure 2 may be further analyzed by considering a few of the key attributes. For example, Figure 3 shows the temperature dependence of the permanent set from these wires after unloading from 6% strain. At lower temperatures, the unresolved strain is due to deformation of the martensite, and can be recovered by heating above $A_f$. The

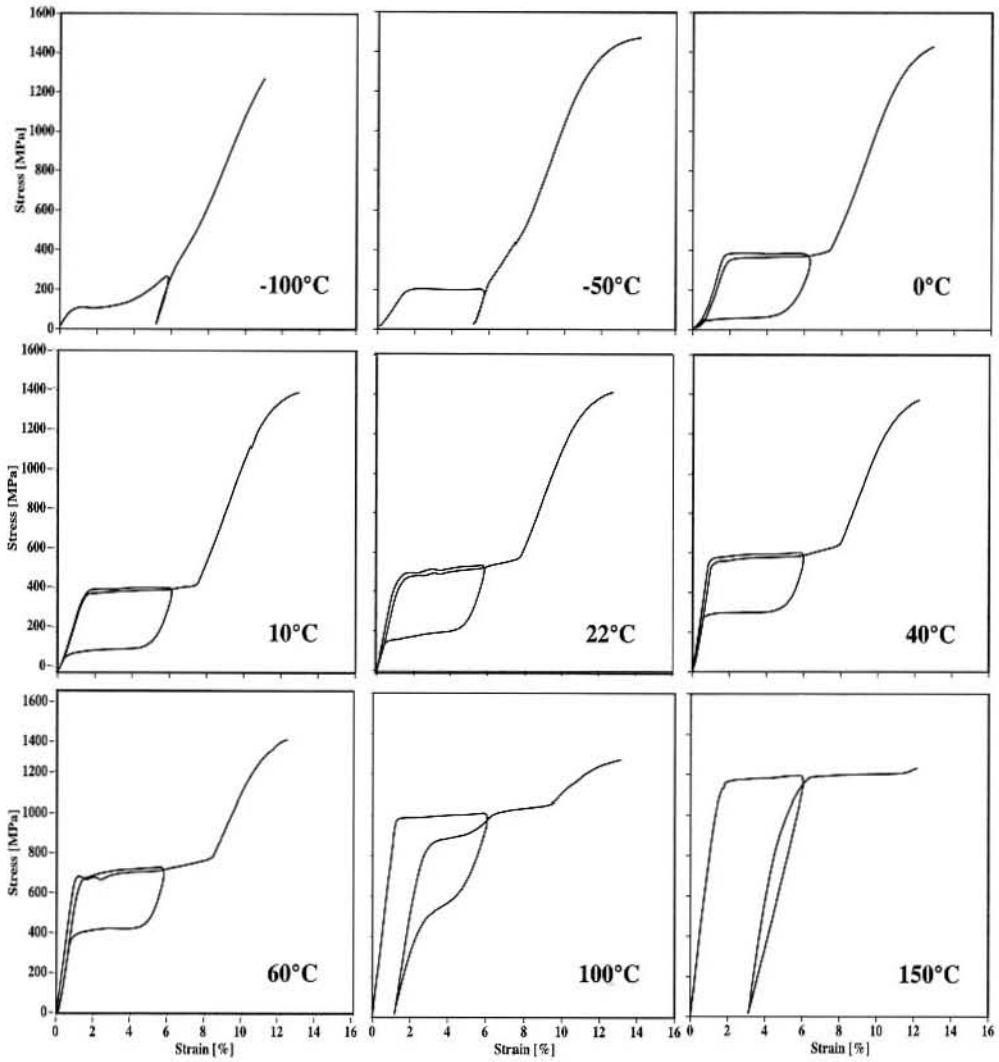


*Figure 2 Effect of test temperature on the mechanical behavior of Nitinol wire. There is a systematic increase in the loading and unloading plateau stresses with increasing test temperature; below 0°C, the structure is martensite and above 150°C the graph shows conventional deformation of the austenite; intermediate temperatures all show classic transformational superelasticity.*

residual strain is nearly zero between 0 and 60°C, which defines the superelastic window for this alloy. As noted above, the non-recoverable plastic strain is about 1% at 100°C and then increases to about 3% at 150°C. Many medical applications require superelastic behavior between room temperature and body temperature. Therefore, this 60°C window is perfectly centered about the intended application range.

Figure 4 shows the effects of test temperature on the loading, unloading, and ultimate tensile stress. We see that there is a linear relationship between plateau stress and temperature between about

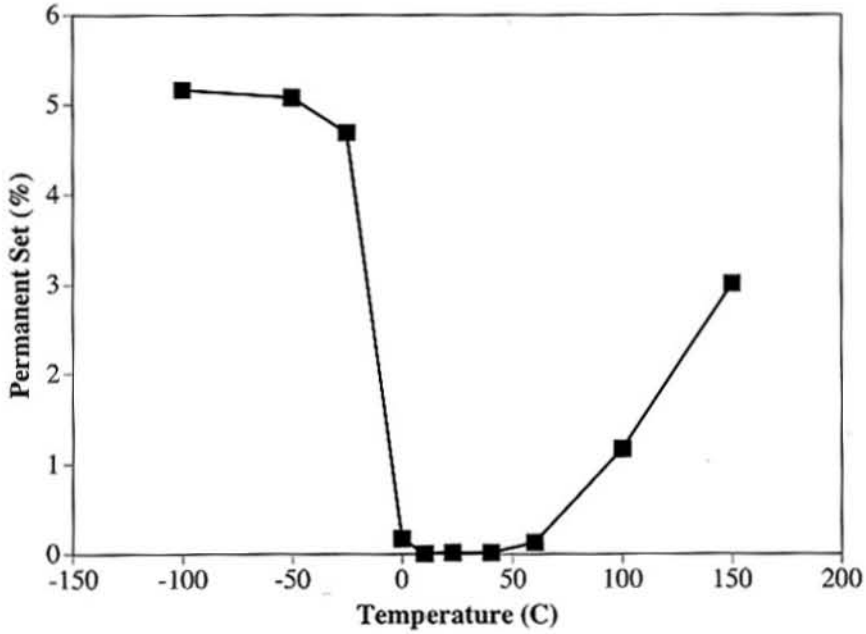


*Figure 3 Effect of test temperature on permanent set. (Note: graph drawn from data in Figure 2; the superelastic window extends from ~ 0–60°C where there is minimal residual strain after unloading from 6% strain; below 0°C, the strain can be recovered by heating above $A_f$ = 11°C, and at higher temperatures the residual strain is due to plasticity).*

0 and 60°C for the unloading plateau and up to 150°C for the loading plateau. These variations in plateau stress follow the Clausius-Clapeyron relationship for a first-order transformation [10]:

$$\frac{d\sigma}{dT} = \frac{-\Delta H}{\varepsilon_O T}$$

Where $d\sigma$ is the change in plateau stress, $T$ is the test temperature, $\Delta H$ is the latent heat of transformation (obtained from DSC measurements), and $\varepsilon_o$ is the transformational strain. $\Delta H$ and $\varepsilon_o$ are controlled by the crystallography of the transformation and can be considered constants. The right side of the equation therefore defines the *stress rate* for the stress-induced transformations. For the present case, the stress rate is 6.1 MPa/°C, which is within the typical range of 3 to 20 MPa/°C for Nitinol alloys [11]. The consequence of this relationship is that the mechanical properties of TiNi alloys depend directly on the transformation temperature and test temperature. The ultimate tensile stress gradually decreases from approximately –100 to 150°C with a slight minimum at 150°C. The UTS and plateau stress converge above this temperature, which is a further indication that $M_d$ is near 150°C.

The initial linear portion of the tensile stress-strain curves in Figure 2 may also be analyzed. The modulus of the wires changes dramatically as the temperature increases from –100 to 150°C, as shown in Figure 5. The implication of these data for guidewire-type applications is that the wires will tend to droop under their own weight at lower temperatures compared with higher stiffness at higher temperatures.

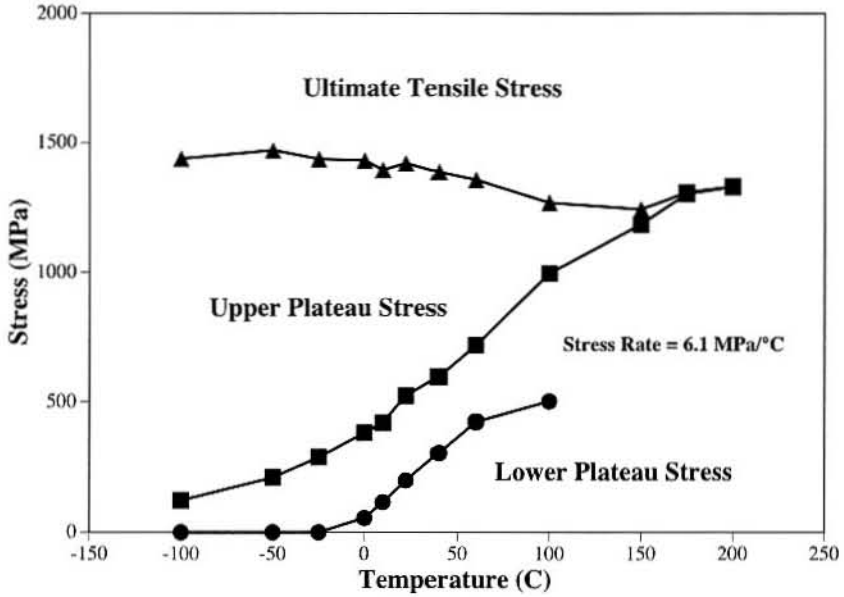


*Figure 4 Effect of test temperature on plateau and tensile stresses is (note: graph drawn from data in Figure 2; there is a linear relationship between plateau stress and test temperature from about 0 to 100°C with a slope, or stress rate, of 6.1MPa/°C; the ultimate tensile stress shows a gradual decrease with increasing temperature with a minimum at the $M_d$ of 150°C).*

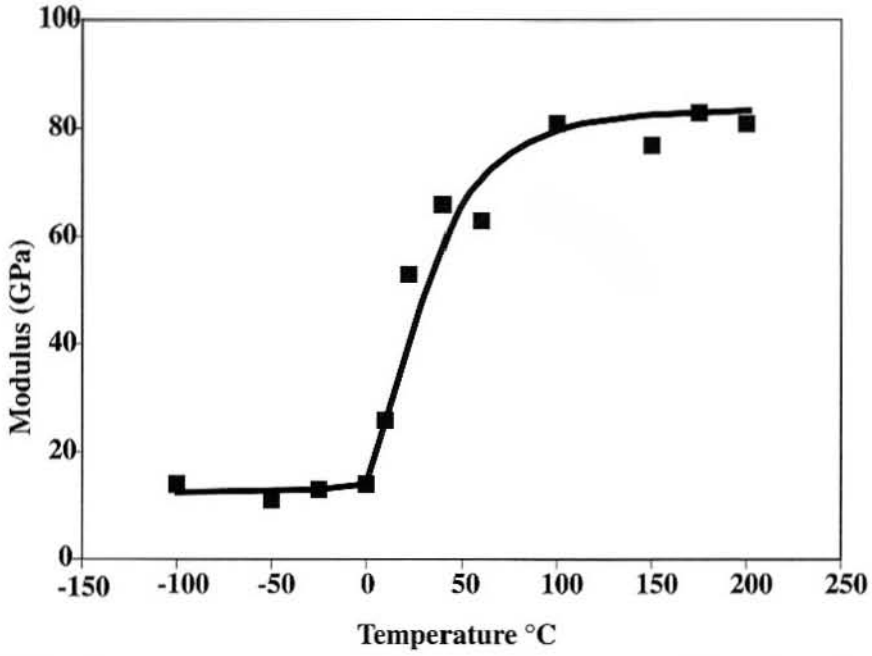


*Figure 5 Effect of test temperature on initial elastic modulus (note: graph drawn from data in Figure 2; note also the precipitous drop in modulus between 100 and 0°C).*

## EFFECTS OF AGING TREATMENTS

Several investigators have shown that optimal superelastic performance can be achieved in Nitinol alloys that have a combination of cold work and aging heat treatments [11,12]. Precise control of these thermomechanical treatments can lead to reproducible mechanical properties and transformation temperatures. TiNi alloys with 50.8% Ni respond well to aging heat treatments to tune in the desired properties. The intent of this section is to provide the background necessary to shape set straight Nitinol wire from the above section into another unique shape.

Nishida, et al. established the effects of aging time and temperature on the TiNi precipitation reactions in Ti-52%Ni alloys by metallographic techniques [13]. They observed precipitation sequence of $Ti_{11}Ni_{14}$-$Ti_2Ni_3$-$TiNi_3$ in the TiNi matrix at temperatures between 500 and 800°C and for times up to 10,000 hours and presented the data in a Time-Temperature-Transformation (TTT) diagram. Their work gave great insight into the metallurgical tool of controlling precipitation reactions in Nitinol alloys. Clearly, however, the times investigated by Nishida, et al. are significantly longer than can be tolerated in a production environment. Therefore, straight wires from the previous section ($A_f$ = 11°C) were aged between 300 and 600°C for 2 to 180 minutes to characterize the effects on transformation temperature and mechanical properties. Figure 6 illustrates these effects on the $A_f$ temperature. We note that the transformation temperature does not change significantly at 300°C. Also, at 500°C, the $A_f$ increases slightly at short times, but does not increase rapidly. The intermediate temperatures, namely 350 to 450°C, have a greater impact on the transformation temperature. At the highest aging temperatures, 500 to 600°C, there is an initial decrease in $A_f$ and then a rapid increase. Admittedly, these trends of temperature and time on the $A_f$ may appear counterintuitive. However, more clarity is gained by grouping the time-temperature conditions to obtain common $A_f$ temperatures. Figure 7 is such a TTT diagram, where each *c-curve* represents the loci

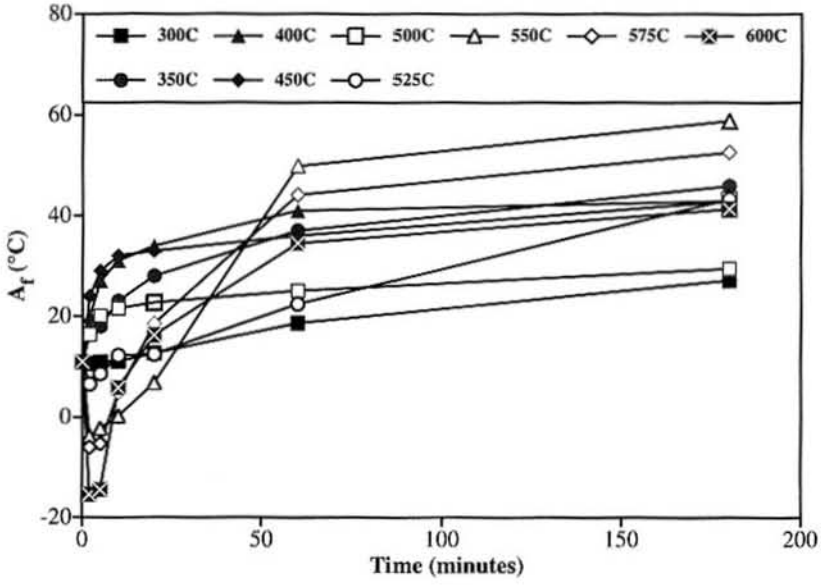


*Figure 6 Effect of aging temperature and time on the transformation temperature of Ti-50.8Ni (at.%) Nitinol wire with a starting $A_f$ temperature of 11°C (note that all of the aging temperatures tend to increase the transformation temperature, although above 500°C there is an initial decrease).*

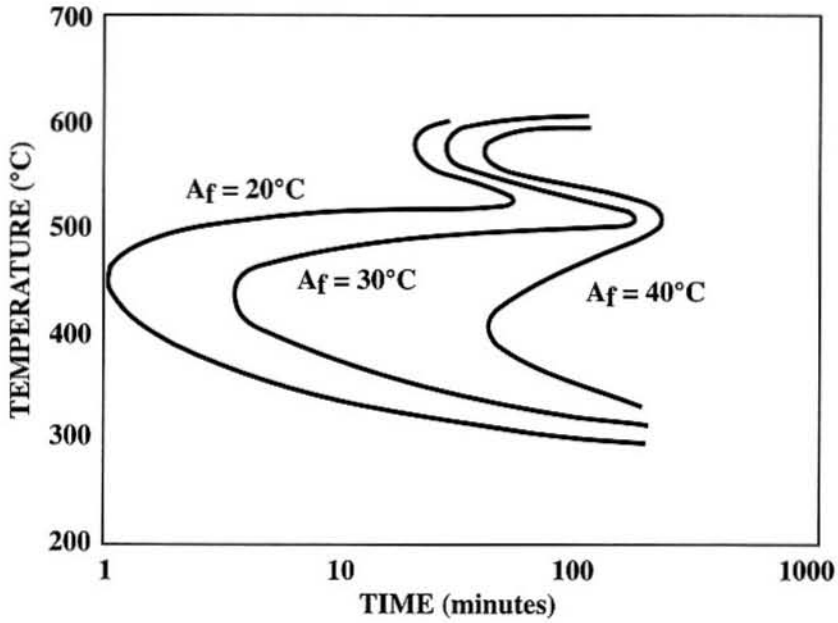


*Figure 7 Effect of aging temperature and time on the transformation temperature of Ti-50.8Ni (at.%) Nitinol wire with a starting $A_f$ temperature of 11°C are shown. The data from Figure 6 are re-plotted to illustrate the conventional TTT diagram; the maximum precipitation rate is at about 450°C; between 500 and 600°C the precipitates dissolve and tend to lower the $A_f$; a new precipitate forms at these higher temperatures.*

of constant $A_f$. This figure illustrates that there is a maximum in the precipitation reaction at about 450°C; i.e., the $A_f$ increases most rapidly after heat treatments at 450°C. For example, at 450°C, the $A_f$ increases from 11°C in the as-straightened wire to 30°C after aging for only 5 minutes. To reach the same 30°C $A_f$ at 500°C takes about 60 minutes and at 300°C the time exceeds 180 minutes.

It is certainly beyond the scope of this article to review the metallurgy of precipitation reactions. However, the shape of these curves can be understood by briefly exploring two factors that govern diffusional nucleation and growth of precipitates [14]. At high temperatures, there is sufficient thermal energy to permit rapid diffusion of Ni and Ti atoms in the matrix. It becomes more difficult for the atoms to form a precipitate nucleus as the temperature increases due to higher atomic mobility. At lower temperatures, however, just the opposite situation occurs: here there are high nucleation rates but low diffusion rates. These two processes are optimized at the intermediate temperatures (350–475°C) to achieve maximum precipitation rates. The $A_f$ change, therefore, is due to relative Ni and Ti atom diffusion, where the Ni atoms congregate in the precipitates and the Ti atoms move to the TiNi matrix phase. As the matrix becomes enriched in Ti, the transformation temperature increases as expected from the relationship of composition on transformation temperature [15]. Although the overall composition of the material remains Ti-50.8%Ni, localized shifts of composition affect the transformation temperatures.

The trends in the TTT curves indicate that a single precipitation reaction ($Ti_{11}Ni_{14}$) occurs in the temperature range from 300 to 500°C. Between 500 and 600°C, however, there are cusps in the $A_f$ curves. Above 500°C, the $Ti_{11}Ni_{14}$ precipitates dissolve, and there is a corresponding decrease in the transformation temperature as the Ni atoms diffuse back into the matrix. At longer times above

500°C, the $Ti_2Ni_3$ phase precipitates, which requires an even greater amount of Ni to diffuse away from the matrix. Precipitation of this phase, therefore, will again increase the $A_f$ but at different reaction rates than for $Ti_{11}Ni_{14}$. These findings are consistent with Miyazaki's microstructural study of Ti-50.6%Ni alloys after aging for 60 minutes at 400, 500, and 600°C [12]. His results demonstrate that the maximum density of $Ti_{11}Ni_{14}$ precipitates is obtained at 400°C.

The effects of the aging treatments on the loading plateau stress are shown in Figure 8. Since the wire was *strain-aged* during the initial processing, these additional aging treatments do not increase the loading plateau. Aging temperatures in the 300 to 500°C range systematically decrease the loading plateau, as we would expect with the increase in $A_f$ temperature. Above 500°C, there is an initial decrease in loading plateau stress and then a more rapid decrease as aging and annealing processes occur. The effects of aging on the UTS are more interesting, as seen in Figure 9. Here the aging treatments between 300 and 450°C increase the UTS. This illustrates that the $Ti_{11}Ni_{14}$ precipitates are effective barriers to dislocation motion and act to strengthen the matrix. Although we know that precipitates form during aging above 500°C, there is a dramatic decrease in UTS, especially at 600°C. The decrease in plateau and tensile stress at these higher temperatures reflects that this is an effective temperature range for annealing (dislocation annihilation).

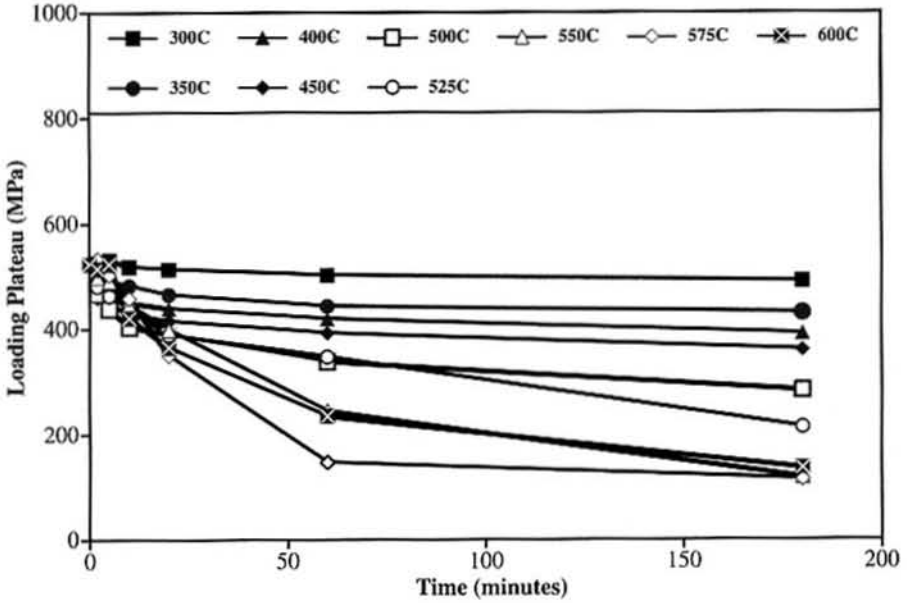


*Figure 8 Effect of time and temperature on the loading plateau of aged Ti-50.8Ni (at.%) alloy. These stress data correspond to the $A_f$ temperatures shown in Figures 6 and 7; there is a systematic decrease in plateau stress with increasing temperature; there is a more dramatic effect above 550°C.*

The above aging discussion points out that the transformation temperature can be readily adjusted by selecting an appropriate time and temperature. Higher $A_f$ temperatures are achieved by aging in the 300 to 500°C range. Additionally, the $A_f$ can be lowered by short aging times between 500 and 600°C due to resolutionizing of the precipitates. It should be noted that the exact times and temperatures to achieve a particular transformation temperature may need to be adjusted to accommodate fixture mass and furnace conditions.

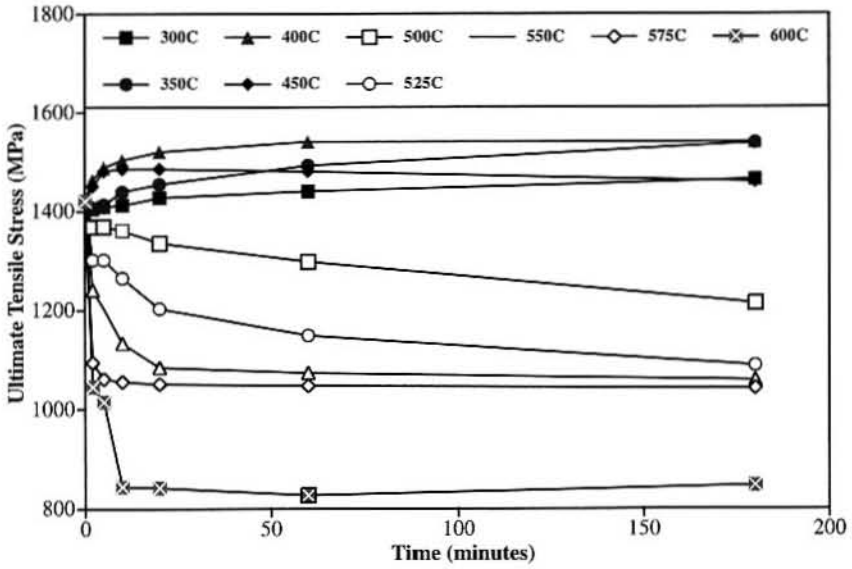


*Figure 9 Effect of time and temperature on the ultimate tensile stress. Aging temperatures between 350 and 450°C tend to increase the tensile strength due to precipitation hardening; between 500 and 600°C, annealing effects dominate and lower the strength.*

## FATIGUE PROPERTIES

Fatigue life is a major concern for biomedical implant applications. For example, the U.S. Food and Drug Administration requires proof of fatigue resistance of 10 years (400 million cycles) in simulated body environment for intravascular stents [16]. Pedersen, et al. measured 6% average diametral strain in proximal aorta at 100 mmHg pressure differential [17]. Therefore, an implanted device could be exposed to pulsatile strains as high as 6% for a 10-year implantation period. The actual mean strain to which the implant is subjected depends on material and design factors. However, whether the stent is manufactured from woven wire, etched sheet, or laser-cut tubing, the strut sections undergo cyclic bending deformation. Furthermore, many Nitinol medical products are tested under accelerated pulsatile conditions that allow only periodic observations to ensure that the devices have survived [18]. A logical approach, however, may be to supplement these submission tests with more fundamental bend-fatigue studies on wires or stent elements [19–23]. The purpose of the present section, therefore, is to review the effects of strain amplitude, stress, and test temperature on the fatigue life of binary TiNi alloy wires.

Miyazaki and co-workers tested cold-worked and aged Ti-50.9Ni and Ti-50.0Ni (at.%) wires in a rotary-bend apparatus [17,19,20]. The specimens were fixed in a bent shape with a suitable radius of curvature to induce a desired strain at the specimen surface at test temperatures above and below $A_f$. Figure 10 shows the (outer fiber) strain amplitude ($\varepsilon_a$) versus the number of rotations to fracture ($N_f$) relationship at each test temperature for the two alloys. The upper diagram presents three curves for the Ti-50.9at.%Ni alloy and the lower diagram shows the data for the Ti-50.0Ni (at.%) alloy. Both alloys show a general trend of increasing fatigue life with decreasing test temperature in the high-cycle fatigue regions (high and intermediate strain-amplitude regions). In the higher Ti alloy, the fatigue endurance limit increases with decreasing temperature below $A_f$. The fatigue limit is insensitive to temperature for the Ti-50.0Ni (at.%) alloy above $A_f$ and for all conditions for the Ti-50.9Ni.

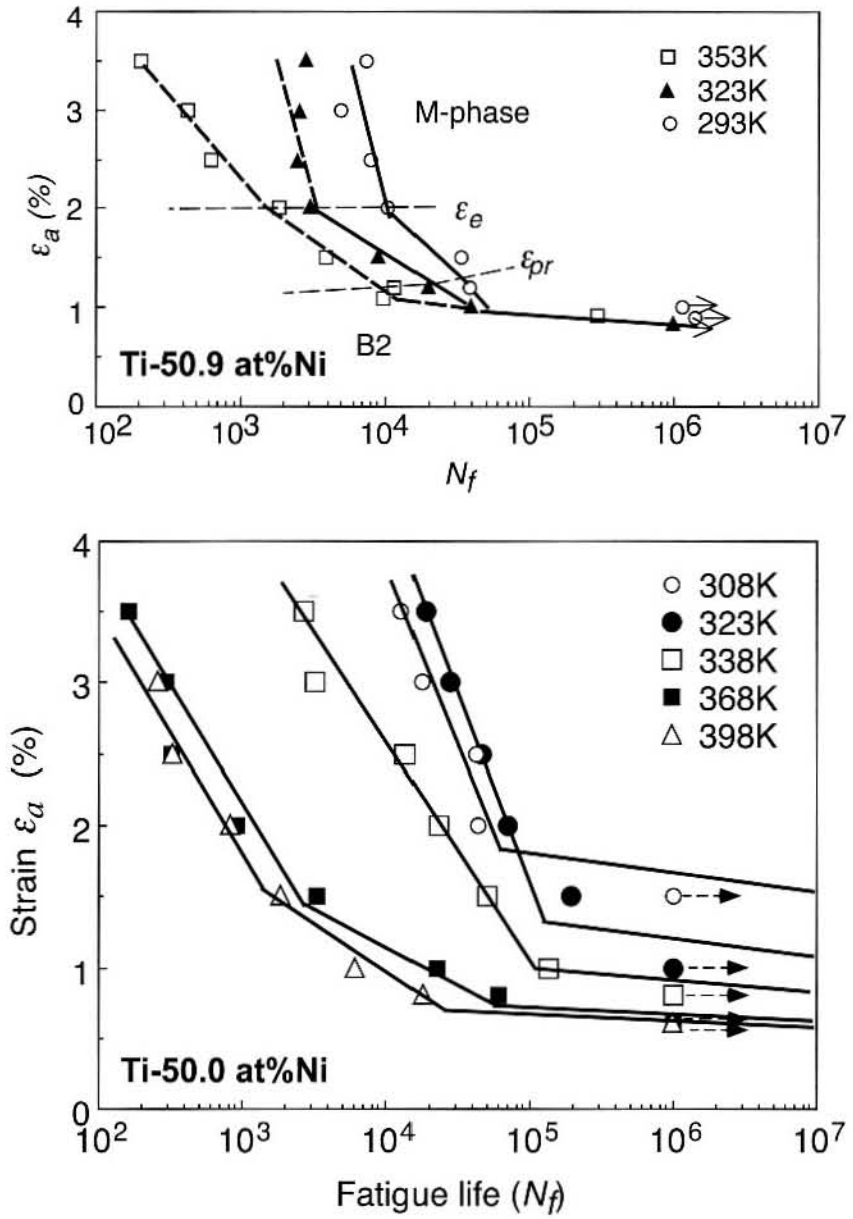


*Figure 10 Effect of applied strain on the rotary bending fatigue life for Ti-50.9Ni (top) and Ti-50.0Ni (at.%) (bottom) alloys at various test temperatures; endurance limit tends to increase with decreasing test temperature (after Miyazaki, et al.).*

Miyazaki, et al. carefully studied the details of tensile stress-strain curves to gain insight into the fundamental mechanisms that influence fatigue behavior and give rise to the differences observed in Figure 10 [20]. They measured the proportional stress limit ($\sigma_{pr}$) and the critical stress to induce the martensitic transformation ($\sigma_M$) as well as the corresponding strains as schematically illustrated in Figure 11. Below the proportional limit strain ($\varepsilon_{pr}$), there is pure elastic deformation; whereas,

between $\varepsilon_{pr}$ and the elastic limit strain ($\varepsilon_e$), there is anelastic deformation including microscopic local twinning or microscopic local stress-induced transformation. The authors further note that the difference between $\varepsilon_{pr}$ and $\varepsilon_e$ is small below $A_f$ and increases with increasing temperature above $A_f$, especially for the Ti-50.0Ni (at.%) alloy.

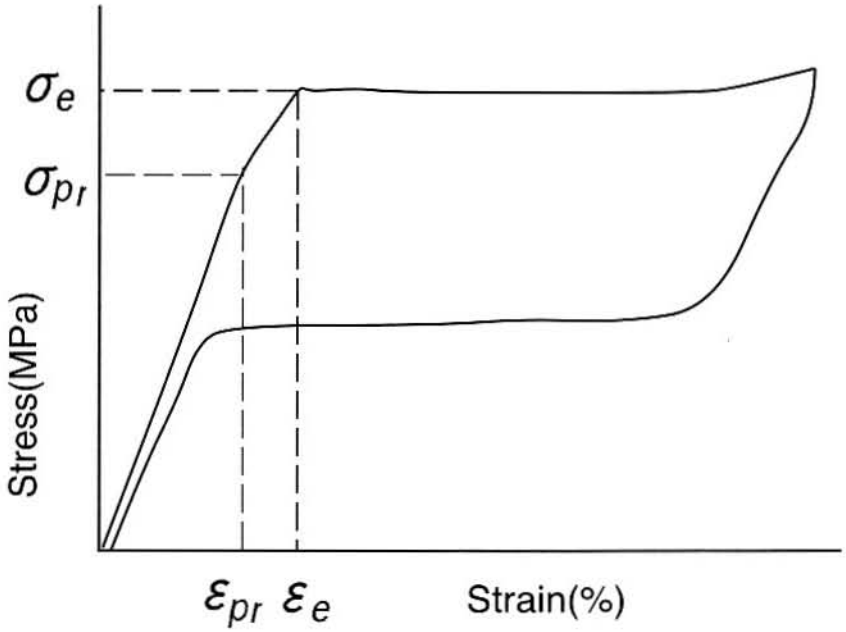


*Figure 11 Schematic stress-strain curve of a superelastic TiNi alloy that illustrates the proportional stress limit ($\sigma_{pr}$) and the critical stress to induce the martensitic transformation ($\sigma_M$) and corresponding strains (after Kim and Miyazaki).*

The differences in the fatigue behavior of these wires can be further understood by considering the mechanisms of the phase deformation. Above $A_f$, deformation occurs by stress-induced martensite, which is the most severe among the modes tested. Between $A_s$ and $A_f$, deformation is partial stress-induced martensite and partial twinning of the martensite. Testing just below $A_s$, the first cycle is stress-induced martensite that is followed by twinning of the martensite. At the lowest test temperatures, deformation is accommodated by martensitic twinning. It is interesting that the fatigue-crack propagation behavior of TiNi alloys is also differentiated by the details of the deformation mode. Crack-growth rates are found to be faster and the fatigue threshold values are lower than conventional metallic engineering alloys of comparable strength [24,25]. Dauskardt, et al. and Melton and Mercier observed that fatigue-crack growth rates were much slower in fully martensitic TiNi alloys than in alloys that undergo a stress-induced transformation [24,26].

Rotary bend testing provides data for conditions of zero mean strain with fully alternating cyclic strains. Recent reports of fatigue testing of stent elements include conditions of non-zero mean strains [21–23]. These data indicate that strain endurance limit does not strongly depend on mean strain at a constant test temperature. These trends have profound implications on analysis of device safety factors compared with typical linear-elastic, Goodman-type construction.

## CONCLUSIONS

The goals of this paper were to correlate the properties of TiNi alloys with processing and test temperature. Optimized Ti-50.8Ni (at.%) wire was manufactured according to industry standards by precise control of the composition, cold work, and continuous strain-age annealing. Properties of as-processed wires vary between test temperatures between -100 and 150°C. For the particular thermomechanical processing of the present wire, there is a *superelastic window* between about 0 and 60°C. Aging treatments between 300 and 600°C can be used to tune final transformation temperatures and mechanical properties. It was shown that aging promotes strengthening of the UTS due to precipitation reactions; however, these precipitates were not effective barriers to the martensite-austenite interface. Low-cycle fatigue properties were shown to vary with test temperature for two binary TiNi alloys. However, there is a general trend for nearly constant endurance limits under high-cycle fatigue conditions.

## REFERENCES


1. J. Hunter and J. Sackier, in *Minimally Invasive Surgery*, eds. J. Hunter and J. Sackier (New York: McGraw-Hill, 1993), 3.
2. D. Stöckel, in *SMST-2000: Proceedings of the International Conference on Shape Memory and Superelastic Technologies*, eds. S.M. Russell and A.R. Pelton, (Pacific Grove, California: International Organization on SMST, 2001).
3. T. Frank, W. Xu, and A. Cuschieri, in *SMST-2000: Proceedings of the International Conference on Shape Memory and Superelastic Technologies*, eds. S.M. Russell and A.R. Pelton, (Pacific Grove, California: International Organization on SMST, 2001).
4. T. Duerig, D. Tolomeo, and M. Wholey, in *SMST-2000: Proceedings of the International Conference on Shape Memory and Superelastic Technologies*, eds. S.M. Russell and A.R. Pelton, (Pacific Grove, Calif.: International Organization on SMST, 2001).
5. *Shape Memory Alloys*, ed. H. Funakubo (New York: Gordon and Breach, 1984).
6. *Engineering Aspects of Shape Memory Alloys*, eds. T. Duerig, et al. (London: Butterworth-Heinemann, 1990).
7. A. Schüßler, in *SMST-97: Proceedings of the Second International Conference on Shape Memory and Superelastic Technologies*, eds. A.R. Pelton, et al. (Pacific Grove, California: International Organization on SMST, 1997), 143–148.
8. L. Buchaillot, in *SMST-97: Proceedings of the Second International Conference on Shape Memory and Superelastic Technologies*, eds. A.R. Pelton, et al. (Pacific Grove, California: International Organization on SMST, 1997), 183–186.
9. D. Hodgson and S. Russell, in *SMST-2000: Proceedings of the International Conference on Shape Memory and Superelastic Technologies*, eds. S.M. Russell and A.R. Pelton, (Pacific Grove, California: International Organization on SMST, 2001).
10. K. Shimizu and T. Tadaki, in *Shape Memory Alloys*, ed. H. Funakubo (New York: Gordon and Breach, 1984), 1–60.
11. T. Duerig and R. Zadno, in *Engineering Aspects of Shape Memory Alloys*, eds. T. Duerig, et al. (London: Butterworth-Heinemann, 1990), 369–393.
12. S. Miyazaki, in *Engineering Aspects of Shape Memory Alloys*, eds. T. Duerig, et al. (London: Butterworth-Heinemann, 1990), 394–413.

13. M. Nishida, C. Wayman, and T. Honma, *Met. Trans.* **17A** (1986), 1505–1515.

14. H. Aaronson, Y. Lee, and K. Russell, in *Precipitation Processes in Solids*, ed. K. Russell and H. Aaronson (Warrendale, Pa.: AIME, 1978), 31–86.

15. K. Melton, in *Engineering Aspects of Shape Memory Alloys*, eds. T. Duerig, et al. (London: Butterworth-Heinemann, 1990), 21–35.

16. U.S. Department of Health and Human Services, "Guidance for the submission of research and marketing applications for interventional cardiology devices" (U.S. Department of Health and Human Services, U.S. FDA, 1995).

17. O. Pedersen, A. Aslaksen, and H. Vik-Mo, *J. Vascular Surgery* **17** (1993), 596–601.

18. R. Glenn and J. Lee, in *SMST-97: Proceedings of the Second International Conference on Shape Memory and Superelastic Technologies*, eds. A.R. Pelton, et al. (Pacific Grove, California: International Organization on SMST, 1997), 585–590.

19. Y. Kim and S. Miyazaki, in *SMST-97: Proceedings of the Second International Conference on Shape Memory and Superelastic Technologies*, eds. A.R. Pelton, et al. (Pacific Grove, California: International Organization on SMST, 1997), 473–477.

20. S. Miyazaki, et al., *Mater. Sci. Engin. A* **273–275** (1999), 658–663.

21. D. Tolomeo, S. Davidson, and M. Santinoranont, in *SMST-2000: Proceedings of the International Conference on Shape Memory and Superelastic Technologies*, eds. S.M. Russell and A.R. Pelton. (Pacific Grove, California: International Organization on SMST, 2001).

22. W. Harrison and Z. Lin, in *SMST-2000: Proceedings of the International Conference on Shape Memory and Superelastic Technologies*, eds. S.M. Russell and A.R. Pelton, et al. (Pacific Grove, California: International Organization on SMST, 2001).

23. R. Tablani, N. Simha, and B. Berg, *Mater. Sci. Engin. A* **273–275** (1999).

24. R. Dauskardt, T. Duerig, and R. Ritchie, *MRS Int'l. Mtg. Adv. Mats.* **9** (1989), 243–249.

25. A. McKelvey and R. Richie, forthcoming in the Fall 1998 MRS proceedings.

26. K. Melton and O. Mercier, *Acta Metallurgica* **27** (1979), 137–144.